ROYAL AIRCRAFT ESTABLISHMENT

BEDFORD.

MINISTRY OF AVIATION

AERONAUTICAL RESEARCH COUNCIL

CURRENT PAPERS

The 7in. x 7in. Hypersonic Wind Tunnel at R.A.E. Farnborough

Part IV - Measurements of Diffuser Performance,

Blockage, Starting Loads and Humidity

by

J. F. W. Crane and J. G. Woodley

THE 7 IN. x 7 IN. HYPERSONIC WIND TUNNEL AT R.A.E. FARNBOROUGH
PART IV - MEASUREMENTS OF DIFFUSER PERFORMANCE,
BLOCKAGE, STARTING LOADS AND HUMIDITY

by

J. F. W. Crane
and
J. G. Woodley

SUMMARY

The performance of the diffuser is analysed, (a) for a conventional closed-jet tunnel with a two-dimensional M = 7 nozzle, and (b) for a type of free-jet tunnel resulting from the combination of an axisymmetric M = 8.6 nozzle and a two-dimensional working section.

Some results of model blockage are given together with a new correlation of closed-jet tunnel results.

Starting loads measured on two models show that the load varies with back pressure and may be reduced to insignificant size.

Humidity measurements show that the technique of drying-by-compression is satisfactory.

LIST OF CONTENTS

LIST OF TABLES

LIST OF ILLUSTRATIONS

---

1 INTRODUCTION

This Note is the fourth of a series describing the R.A.E. 7 in. × 7 in. hypersonic wind tunnel. Previous reports have discussed the tunnel design, instrumentation and flow visualisation techniques[1], the heater performance[2], and the calibration[3] of the two-dimensional M = 7 fuzed silica nozzle. The diffuser performance, and measurements of blockage, starting loads, and humidity are described in the present Note.

The combination of a M = 8.6 axisymmetric nozzle and a two-dimensional working section resulted in a type of free-jet tunnel. This "free-jet" tunnel has a very short free-jet, and separated flow regions confined mainly to the four corners of the working section/nozzle junction. It is, therefore, intermediate between the conventional free-jet tunnel with large plenum chamber, and the closed-jet tunnel. Nothing appears to have been written about this type of tunnel so the opportunity was taken of calibrating the diffuser quite extensively.

It was found that (a) the flow transformation[4] from free-jet to closed-jet at the diffuser entrance is accomplished supersonically and not sub-sonically as generally found[4] in conventional free-jet tunnels; (b) blockage is more easily produced with high drag bodies than would be expected with a closed-jet tunnel (see section 3); (c) the pressure recovery, when compared with the pitot recovery at the diffuser entrance, and second throat size minima for starting and running are comparable to those of a closed-jet tunnel; (d) a model in the tunnel is almost as effective as a second throat in improving the pressure ratio requirements for starting.

Examination of data on model blockage in closed-jet tunnels obtained both in this tunnel and elsewhere shows that a reasonable correlation is obtained using a weighting factor of drag coefficient to the half power. A wide range of model shapes is considered including a circular disc which is not correlated by previously published methods[5,6].

Measurements of transient loads on two models during starting and stopping the tunnel show that in general the starting load is the greatest, and that it is no greater than twice the steady load. The magnitude of the excess over the steady load depends on the level of back pressure, and it may be reduced to negligible size by reducing the back pressure sufficiently.

Humidity measurements show that the technique of drying the air by compression only, is adequate to avoid any effects of condensation in the flow.

2 DIFFUSER PERFORMANCE

2.1 Description of the diffuser and test apparatus

Fig.1 shows details of the diffuser and the pitot-rake models used in the investigation of its performance. The diffuser consists of a two-dimensional supersonic diffuser, a short transition section (rectangular to circular cross-section), and finally a 6° total angle subsonic diffuser.

Results at M = 7 are for a closed-jet working section, Fig.1(a), whilst those at M = 8.6 are for a "free-jet" working section, Fig.1(b). In the latter the jet expands freely from a diameter of 7 in. to a rectangular cross-section of 8 in. by 7 in. Thus the free-jet is considerably shorter than that of a conventional free-jet tunnel, and the regions of separated flow are concentrated mainly in the corners of the working section instead of all around the model testing region, hence the identifying quotation marks.

For the M = 7 tests, a pitot rake was mounted in the working section
and failure to start was indicated by vibration of the rake and its support.
For the M = 8.6 tests, which were done both with an empty tunnel and with
models, failure to start, and flow breakdown, were indicated by one or more
of the following, (a) pitot pressure, (b) static pressure at the wall of the
working section, (c) Schlieren observation, (d) diffuser noise.

Mercury manometers were used to measure pressure differences and a
Midwood capsule manometer was used as an absolute reference. Stagnation
pressure in the settling chamber was measured very accurately by a balancing
system[1]. Stagnation temperature was of the order of 400°C.

2.2 Diffuser performance at M = 7 with a closed-jet working section

During the initial calibration of the tunnel with the M = 7 wedge
nozzle, the following limited information on diffuser performance was
obtained. For the configuration, Fig.1(a), with a model in the working
section, and the ratio of 2nd throat area to diffuser entrance area
A_2^*/A_e = 0.65, the ratio of vacuum pressure to stagnation pressure
p_v/p_o = 0.0064 was found to be a maximum for starting. This pressure ratio
is equal to 0.41 times the pitot recovery for M = 7.

Second throat size minima, and the complete characteristics of starting
and breakdown pressure ratios were not measured.

2.3 Diffuser performance at M = 8.6 with a "free-jet" working section

2.3.1 Introduction

In the tunnel arrangement, Fig.1(b), the M = 8.6 axisymmetric nozzle
produces a circular jet which issues freely into a rectangular-section
working section. Tests of a range of models showed that blockage occurred
more readily with this arrangement than would be expected with a closed-jet
working section.

It is shown elsewhere[4] that in a free-jet wind tunnel, in the
majority of cases, the flow is decelerated to subsonic speed at the entrance
to the diffuser by turbulent mixing at the edge of the free-jet. (In a
closed-jet tunnel the flow is supersonic at the entrance to the diffuser.)

To ascertain the diffuser performance of the present somewhat
unfamiliar and unconventional tunnel arrangement a rather comprehensive
series of tests was made at this Mach number.

2.3.2 Calibration of the expanding jet

Examination of the jet in its transformation from circular to
rectangular cross-section was made with a single pitot tube, and a single
5° cone/cylinder static pressure probe, both inserted from the sidewall, and
by a pitot rake mounted on a sting.

Fig.2(a) shows pitot pressure profiles across the horizontal centreline
at 3 stations (see Fig.1(b)). At station 1, the model testing region, there
is a 4 in. diameter core of uniform flow at M = 8.6 with no transformation
effects apparent. Profiles on other diameters at this station are similar.

At station 2, the axis of the downstream window, the uniform core is
reduced to 2 in. in diameter by the influence of the transformation.

At station 3, at the entrance to the diffuser, the jet is now fully expanded, but some recompression is occurring at a radius of $2\frac{1}{2}$ in. The average pitot pressure at this station is $p_0'/p_0 = 0.0039$ or 64 per cent of the pitot recovery at station 1.

Fig.2(b) shows the static pressure profile at station 2. This profile confirms that the transformation is supersonic, and this is the general case. The static pressure at the centreline of the tunnel is higher than would be expected for the Mach No. deduced from the p_0'/p_0 ratio, but this may be due to (a) the inaccuracy of measurement at this extreme and of the Midwood manometer range, or (b) the effect of air liquefaction which may have occurred. With regard to the latter, it has been shown [9] that even a very large degree of liquefaction has negligible effect on diffuser performance at this Mach number level.

2.3.3 Static pressure measurements at the downstream window of the working section, station 2

Plots of the variation of static pressure measured at the wall of the working section, p_w, with back pressure, p_v, are given in Fig.3. Fig.3(a) shows that, for an empty tunnel with $A_2^*/A_e < 0.535$, p_w remains constant with increase in p_v up to a level just below that of the average pitot pressure at the diffuser entrance. The change in flow pattern at breakdown produces a fairly rapid rise in p_w.

For an empty tunnel with no second throat, $A_2^*/A_e = 1.136$, the change in flow pattern occurs much earlier, at p_v equal to about one third of the pitot pressure at the diffuser entrance, and the rate of increase of p_w with p_v is small. This breakdown was accompanied by a low-pitched noise from the diffuser, the noise level increasing with increase in p_v. The mechanism of breakdown was not investigated, but it appears to be a very gradual process in this case.

Fig.3(b) shows plots of p_w versus p_v for the tunnel with a model, for various second throat sizes. There is a general improvement in the performance of the diffuser over that of the empty tunnel, and the premature breakdown for the condition of no second throat was not experienced.

2.3.4 Minimum second throat size for starting

The minimum second throat sizes for starting for an empty tunnel and for a tunnel with a model were measured and found to be:-

For an empty tunnel, $A_2^*/A_e = 0.495$ at $p_0 = 750$ psig.

For a tunnel with model, $A_2^*/A_e = 0.527$ at $p_0 = 750$ psig,

and $A_2^*/A_e = 0.54$ at $p_0 = 400$ psig. The difference between the latter two measurements is probably due to the change in boundary layer thickness in the diffuser with change in p_0.

A simple one-dimensional theory, commonly used to predict the minimum second throat size for starting, which assumes a normal shock at the diffuser entrance and sonic speed at the second throat (normal shock swallowing

function[4]), gives $A_2^*/A_e = (A_1^* p_0/A_e p_0')_{M = 8.6} = 0.616$, a value which is 12 to 20 per cent greater than the experimental results. With this simple theory $A_2^*/A_e \to 0.6$ as $M \to \infty$ so that the dependence on M is negligible and the effect of the transformation on the Mach No. at the diffuser entrance may be ignored.

These results are in general agreement with published data[4,9] for closed-jet tunnels of similar Mach number.

2.3.5 Minimum second throat size for running

The minimum second throat size for running was not attained because of mechanical limitations. From the present results and from the data of similar tunnels[4,9], it is likely to lie in the range $0.1 < A_2^*/A_e < 0.25$.

2.3.6 Maximum starting and flow breakdown pressure ratios

Fig.4(a) shows that, for an empty tunnel without a second throat, the maximum pressure ratio for starting is $p_v/p_0 = 0.00105$. This is considerably smaller than the maximum found for an empty tunnel with an automatic (in which the second throat is fully open at the start and is closed to the run position by an actuating piston which draws its air supply from the settling chamber), and hence optimum, second throat which is $p_v/p_0 = 0.00285$. Breakdown pressure ratio is somewhat greater than the maximum starting pressure ratio and has a maximum of $p_v/p_0 = 0.0036$ at $A_2^*/A_e = 0.25$.

Fig.4(b) shows that for a tunnel with a model in the working section, the maximum starting pressure ratio with no second throat is $p_v/p_0 = 0.00265$, which is a considerable improvement on the empty tunnel result and shows that a model is quite as effective as a fixed second throat. The breakdown pressure ratio characteristic also shows some improvement over that of an empty tunnel, and the maximum value of $p_v/p_0 = 0.0048$ at $A_2^*/A_e = 0.25$ is about $1\frac{1}{4}$ times the average pitot recovery at the diffuser entrance.

2.3.7 Effect of stagnation pressure on breakdown pressure ratio

Fig.5(a) shows the effect of stagnation pressure on the breakdown pressure ratio for the tunnel with a model (pitot rake). The model was positioned 6 in. upstream of the nozzle exit, Fig.1(b), and flow breakdown was determined from the pitot pressure profile. The characteristics show that for a drop in p_0 from 750 psig to 400 psig there is a drop in pressure recovery of 3 per cent over most of the range with a maximum of 12 per cent at $A_2^*/A_e = 0.25$.

2.3.8 Comparison of breakdown pressure ratio characteristics for different tunnel arrangements

Fig.5(b) compares the breakdown characteristics at $p_0 = 750$ psig for various tunnel arrangements. In general, the "free-jet" tunnel with a model has a better pressure recovery than an empty tunnel, and a better recovery is obtained with a model in the nozzle compared with one mounted in the working section further downstream. The latter result may be associated with the gradual nature of the breakdown process. (It should be noted that optimum recoveries were not determined because the optimum second throat sizes were unobtainable due to mechanical limitations.)

2.3.9 Model blockage in a "free-jet" tunnel

Model blockage characteristics of a "free-jet" tunnel are distinctly different from those of a closed-jet tunnel (see section 3). High drag bodies, for example, models 5 and 7 of Table 1 which did not cause blockage in the closed-jet tunnel at $M = 6.8$, blocked the flow in the "free-jet" tunnel. Further, a circular disc of only 1.125 in. in diameter blocked the flow in the "free-jet" tunnel.

A number of low drag bodies, however, were successfully tested in the "free-jet" tunnel. Representative of these was a half-cone (14° semi-angle) of 5 in. chord, and $2\frac{1}{2}$ in. span, which was tested at incidences of up to 30°. The addition of a delta wing of $3\frac{3}{4}$ in. span to this model, however, caused blockage at the smaller incidence of 24°.

2.3.10 Conclusions on "free-jet" tunnel diffuser performance

In a free-jet tunnel of this type the flow transformation results in completely supersonic flow at the diffuser entrance, rather than the more general subsonic flow found in conventional free-jet tunnels.

The minimum second throat size for starting is between 80 and 88 per cent of that predicted by a simple theory for swallowing a normal shock.

The minimum second throat size for running was not attained, but it probably lies in the range $0.1 < A_2^*/A_c < 0.25$.

The maximum pressure ratio for starting is $p_v/p_o = 0.00285$ or 73 per cent of pitot recovery at the diffuser entrance.

Optimum breakdown pressure ratio was not attained, but the maximum realised was $p_v/p_o = 0.0048$ at $A_2^*/A_c = 0.25$ or $1\frac{1}{4}$ times pitot recovery at the diffuser entrance, with a model. However, with an empty tunnel with no second throat breakdown occurred at a considerably lower pressure ratio.

The "free-jet" tunnel was found to be very sensitive to model bluntness and blockage occurred readily with high drag shapes, so that testing was confined to low drag shapes. To remedy this defect in the tunnel's performance a conical fairing is to be fitted at the nozzle exit to eliminate the regions of separated flow.

3   MODEL BLOCKAGE IN CLOSED-JET TUNNELS

At present there is no accurate theoretical method of predicting, for a particular model, wind tunnel and Mach number, the maximum possible model size which will not block the flow. Generally, the maximum model cross-sectional area is determined in the following manner (analogous to the method used to predict the minimum second throat size for starting for a diffuser).

As a rough average for the complex starting process, an entropy increase in the flow appropriate to a normal shock wave upstream of the model is postulated, followed by isentropic flow with sonic conditions at the maximum model section. For slender, low drag shapes a maximum of 60 per cent of this theoretical area is generally allowable. For high drag shapes a somewhat smaller percentage must be taken.

3.1   Correlation of blockage results

In order to study possible correlations of the results on blockage for low and high drag shapes, further analysis has been made of some results

which were obtained by Schueler[5] for a range of cones and discs. This analysis showed that at a fixed Mach number the maximum area to avoid blockage for each model was approximately inversely proportional to the half power of its drag coefficient based on base area. Therefore, assuming that this property is also true for other shapes, this suggests that drag coefficient to the half power should prove to be a useful weighting factor, for comparing various types of model, in the standard plots of the ratio of maximum cross-sectional area to the area of the test section versus Mach number.

A plot of this type is given in Fig.6, where the actual results obtained by Schueler are plotted. As can be seen the correlation factor is effective in collapsing results, from such dissimilar models as a sharp 30° total-angle cone and a disc, into a definite band.

This band of results is also illustrated in Fig.7, where it is compared with some results from Ref.6. In these latter results the drag coefficient for each model has been interpreted as the drag coefficient for the part of the body up to its maximum cross-section. Assuming that the trends shown in this figure are also applicable for higher Mach Nos., the curve representing the lower limit of Schueler's results has been extrapolated up to a Mach number of 7.

3.2 Comparison of trend of blockage results with R.A.E. results

At the higher end of the Mach number range the extrapolated curve in Fig.7 serves as a useful comparison with some results obtained at a Mach number of 6.8 in the R.A.E. hypersonic tunnel. A complete list of these results is given in Table 1. Of the models tested only a few were close to the permissible optimum size, and of these in only two cases was the blockage in fact marginal.

One of these was for a model of hyperbolic profile, which was seen to block the tunnel when a small pitot tube was placed close to it. The other was a blunted cone of 90-degrees total angle, which blocked the tunnel only on occasions when starts were attempted with the tunnel walls hot due to previous testing. This effect was caused by a decrease in the effective test section area due to increased thickening of the boundary layer on the hot walls, whereas for the hyperbolic model the blockage was caused by increases in the effective model cross-sectional area and drag coefficient.

Hence in only these two cases is the comparison with the trends deduced from Schueler's results strictly valid, and, as can be seen in Fig.7, for these cases the agreement is quite good.

4 STARTING LOADS

4.1 Description of models and test apparatus

A two-component strain gauge balance, Fig.8(a), and two models Fig.8(b) and (c) were used for starting load tests. These were mounted on a traverse sting which had slight backlash between the racked sting and its driving pinion and guide. Preliminary runs were made with a cone-cylinder-flare model and the temperature of the sting was monitored. It was found that runs of 15 seconds could be made before the effects of convective heat transfer to the model were transmitted to the balance. Hence all subsequent runs were made shorter than 15 seconds and the balance was allowed to cool to some equilibrium temperature before further runs were made. Calibration of the balance at two different levels of temperature showed that the balance calibration constants changed very little over the range of temperature covered by the tests.

The outputs from the two bridges, which were D.C. energised by lead/acid accumulators, were recorded on fast response galvanometers[7], Fig.9.

To ensure that the galvanometer was picking up the initial pulse the signal was checked with a Tektronix oscilloscope and the shape of the trace was found to be similar. The natural frequencies of the two models were 44 c/s for the delta wing and 30 c/s for the cone-cylinder-flare.

4.2 Description of the starting process

Initially, the air surrounding the model is at rest and has a pressure equal to p_v. To start the flow the quick-acting-valve is opened and high pressure air enters the settling chamber. The normal shock preceding this air processes the residual air and enters the diffuser. When the starting pressure ratio is reached $(p_v/p_o = 0.0064$ at $M = 7)$ hypersonic flow is established around the model if the blockage criterion is satisfied.

The time taken for the starting process, therefore, depends on the speed of opening of the quick-acting-valve and the initial pressure in the working section. Measurements of the pressure in the settling chamber with a fast response transducer give time constants of 20 milliseconds for the rise in pressure on opening the quick-acting-valve, and 600 milliseconds for the decay in pressure on closing the valve.

If the flow starts symmetrically then the significant load on the model producing bending in the strain-gauged sting, the normal force Z, increases only with increase in dynamic pressure. Depending on the rate of increase of dynamic pressure and the inertia of the model and sting, the peak load will be no greater than twice the final steady load (see, for example, Ref.8 on the deflection of a cantilever produced by a suddenly applied load).

4.3 Results of starting load measurements

Runs were made at two values of incidence, nominal zero and 4 degrees. The vacuum tank pressure varied between 0.05 atmos. and 0.22 atmos.

Fig.10 shows typical traces of model loading during a short run. At the high value of $p_v = 0.2$ atmos., Fig.10(a), there was an initial kick which produced a strain equal to almost twice the steady load. Damping produced a steady load after about two seconds. Closing of the quick-acting-valve is denoted by a dip in the loading trace and flow breakdown is shown by a pulse, the peak of which is slightly lower than the steady load.

Fig.10(b) shows the effect of a much lower initial pressure $(p_v = 0.05$ atmos.) on the model loading. In this case the starting load is less than the steady load, presumably because the flow is established at a lower stagnation pressure. Damping time is unchanged but the stopping load is indistinguishable on the trace.

Fig.11 shows the effect of p_v on the starting and stopping loads for both models. The normal force coefficient C_Z for starting and stopping increases with increase in the pressure ratio (p_v/p_o). At 4 degrees incidence and at pressure ratios less than about 0.1 times the maximum allowable for starting $(p_v/p_o)_{max. starting}$, the starting load is smaller than the steady load. At higher pressure ratios the starting load was greater than either the steady load or the stopping load, but the peak loading did not exceed twice the steady load, and the high loads were obtained with high values of p_v which would not normally be used in this

tunnel. The small magnitude of the starting load and its reduction with the lowering of p_v allows models to be set at incidence prior to starting, and greatly alleviates the problems of balance design.

Later experience with axisymmetric models has shown that the tunnel can be started with models set at incidences of up to 30°, where the stress in the balance produced by the steady load has been 30 per cent of the yield stress, and no permanent strain of the balance due to starting loads has been detected.

4.4 Conclusions on starting loads

The starting process of this tunnel is very rapid. Measurements of normal force and pitching moment on a delta wing and a cone-cylinder-flare show that:-

(1) At zero incidence the starting load is negligible.

(2) At four degrees incidence, with the pressure ratio (p_v/p_o) less than 0.1 $(p_v/p_o)_{max.\ starting}$, the starting load is less than the steady load.

(3) At four degrees incidence, with the pressure ratio greater than 0.1 $(p_v/p_o)_{max.\ starting}$, the starting load is greater than either the steady load or the stopping load and it increases with increase in pressure ratio. The starting load did not, however, exceed twice the steady load, even at the abnormally high pressure ratio of 0.6 $(p_v/p_o)_{max.\ starting}$.

(4) Experience has shown that the tunnel may be started with models at high incidence without causing permanent strain of the balance.

5 HUMIDITY MEASUREMENTS

The air supply to the tunnel is dried by the process of compression and subsequent cooling, and the condensate is removed both at the interstage drains of the compressors and at the oil/water separators. A valve ensures that the discharge of air into the storage system does not take place if the pressure in the separators is less than 3000 p.s.i.

Measurements of humidity listed in Table 2, made in fact before the installation of this valve, show that moisture which had condensed in the storage system had not been entirely removed by draining. The air, however, was sufficiently dry to avoid condensation effects on the flow in the tunnel.

LIST OF SYMBOLS

A plan area of model

A_e diffuser entrance area

A_m maximum cross-sectional area of model

A_T aerodynamic test section area (geometric test section area minus boundary layer displacement area)

A_2^* supersonic diffuser throat area

C_D drag coefficient $\left(\dfrac{drag}{q\ A_m}\right)$

C_Z normal force coefficient $\left(\dfrac{Z}{q\,A}\right)$

M Mach No. in working section

M' pitching moment

Z normal force

p static pressure

p_0 settling chamber pressure

p_0' pitot pressure

p_v vacuum tank pressure

p_w static pressure at the wall in the working section

q dynamic pressure

α model incidence

LIST OF REFERENCES

Ref. No.	Author	Title, etc.
1	Crabtree, L.F. Crane, J.F.W.	The 7 in. × 7 in. hypersonic wind tunnel at R.A.E. Farnborough. Part 1 – Design, instrumentation and flow visualization techniques. A.R.C. C.P.590. August, 1961.
2	Crane, J.F.W.	The 7 in. × 7 in. hypersonic wind tunnel at R.A.E. Farnborough. Part 2 – Heater performance. A.R.C. C.P.590. August, 1961.
3	Crane, J.F.W.	The 7 in. × 7 in. hypersonic wind tunnel at R.A.E. Farnborough. Part 3 – Calibration of the flow in the working section. A.R.C. C.P.590. August, 1961.
4	Hermann, R.	Supersonic inlet diffusers and introduction to internal aerodynamics. Minneapolis Honeywell Regulator Co. Minneapolis, U.S.A. 1956.
5	Schueler, C.J.	An investigation of the model blockage for wind tunnels at Mach Nos. 1.5 to 19.5. Arnold Engineering Development Center. Tech. Note 59-165, February, 1960.

LIST OF REFERENCES (CONTD)

Ref. No.	Author	Title, etc.
6	Dayman, B. Jr.	Blocking in the supersonic wind tunnel. Jnl. Aero. Sci. $\underline{25}(4)$ April, 1958, 264.
7	Couper, J.E.	The operation and maintenance of Recorder type IT.3-13-61. R.A.E. Instruction Leaflet No. IT.2034. August, 1956.
8	Salmon, E.H.	Materials and Structures. Vol.1, p.276. Longmans, Green & Co. 1931.
9	Wegener, P.P. Lobb, R.K.	NOL hypersonic tunnel No.4 results II. Diffuser investigation. NAVORD Report 2376. P.41711.

TABLE 1

Details of various types of model which have been tested in
the hypersonic tunnel at a Mach No. of 6.8

No.	Model	Length (In.)	Base dia. (In.)	$\frac{A_M}{A_T}$ (A_T = 43 sq. in.)	$\frac{A_M}{A_T} \times C_D^{\frac{1}{2}}$	Flow condition (M = 6.8)
	Conic sections: $y^2 = 2\,Rx + Bx^2$					
1	Hemisphere B = 1.0", R = 1.25"	1.25	2.5	0.114	0.109	Established
2	Hyperbola B = -0.671", R = 0.5"	1.23	3.0	0.164	0.167	Established (Marginal)
3	Ellipse B = 2.0", R = 2.0"	3.0	2.83	0.146	0.162	Established
4	15° total-angle sharp cone	15.2	4.0	0.292	0.060	Established
5	1/10 power law body	3.0	2.23	0.091	0.080	Established
6	$\frac{1}{3}$ power law body	3.38	3.0	0.164	0.107	Established
7	$\frac{1}{2}$ power law body	2.25	3.0	0.164	0.118	Established
8	90° total-angle blunted cone	0.99	3.0	0.164	0.182	Established (Marginal)
9	90° total-angle blunted cone	0.94	3.25	0.193	0.219	Blocked
10	Disc	—	3.0	0.164	0.222	Blocked

TABLE 2

Humidity measurements

Date	Storage pressure (psig)	Dew point temperature (°C)	Absolute humidity (lb/lb)	Relative humidity (Referred to room temp. 15°C)	
-/10/59	3000	-29	0.00031	4.4	Downstream of heater
-/10/59	3000	-40	0.000076	1.1	
-/10/59	3000	-40	0.000076	1.1	
29/ 9/59	3000	-21	0.00057	8.2	
28/ 9/59	1500	-29	0.00026	1.9	
28/ 9/59	1500	-35	0.00014	1.0	Upstream of heater
28/ 9/59	1500	-38	0.0001	0.72	
29/ 9/59	2300	-31	0.00021	2.3	
29/ 9/59	2900	-28	0.00028	3.9	
29/ 9/59	3000	-34	0.00015	2.1	
29/ 9/59	3000	-31	0.00021	3.0	
29/ 9/59	3000	-31	0.00021	3.0	

(a) M = 7 (CLOSED-JET WORKING SECTION.)

AIR FLOW
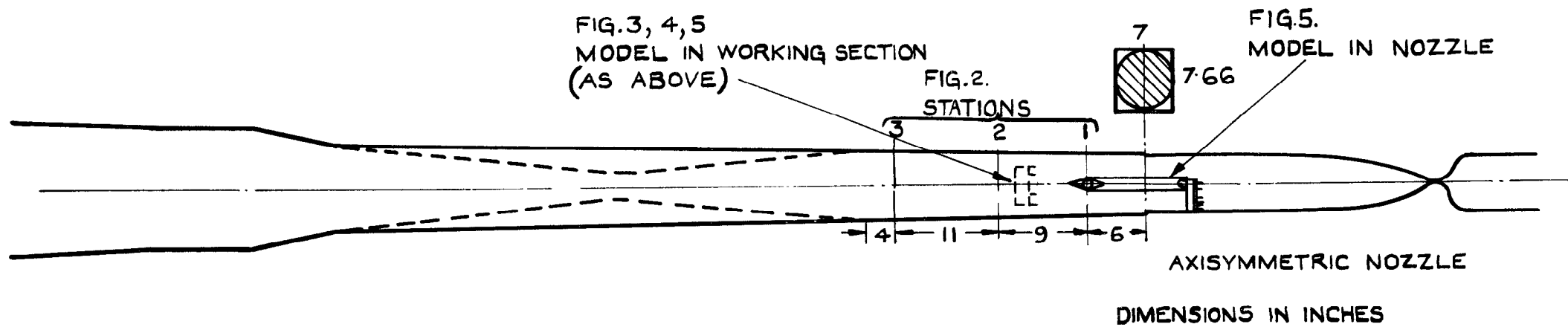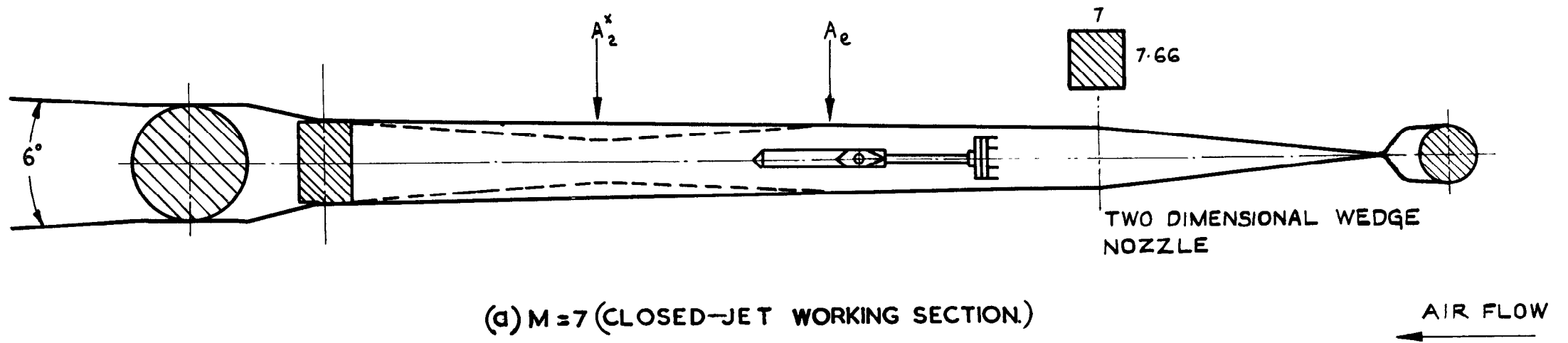
(b) M = 8·6 ("FREE-JET" WORKING SECTION.)

DIMENSIONS IN INCHES

FIG.I. TUNNEL ARRANGEMENTS.

STATION
1 UPSTREAM WINDOW
2 DOWNSTREAM WINDOW
3 DIFFUSER ENTRANCE

$A_2^x/A_e = 1.136$

$p_v/p_0 < 0.001$

PORT WALL

STBD WALL

P_0^1/P_0
$\times 10^4$

r (INCHES)

(a) PITOT PRESSURE PROFILES

P/P_0
$\times 10^4$

PORT WALL
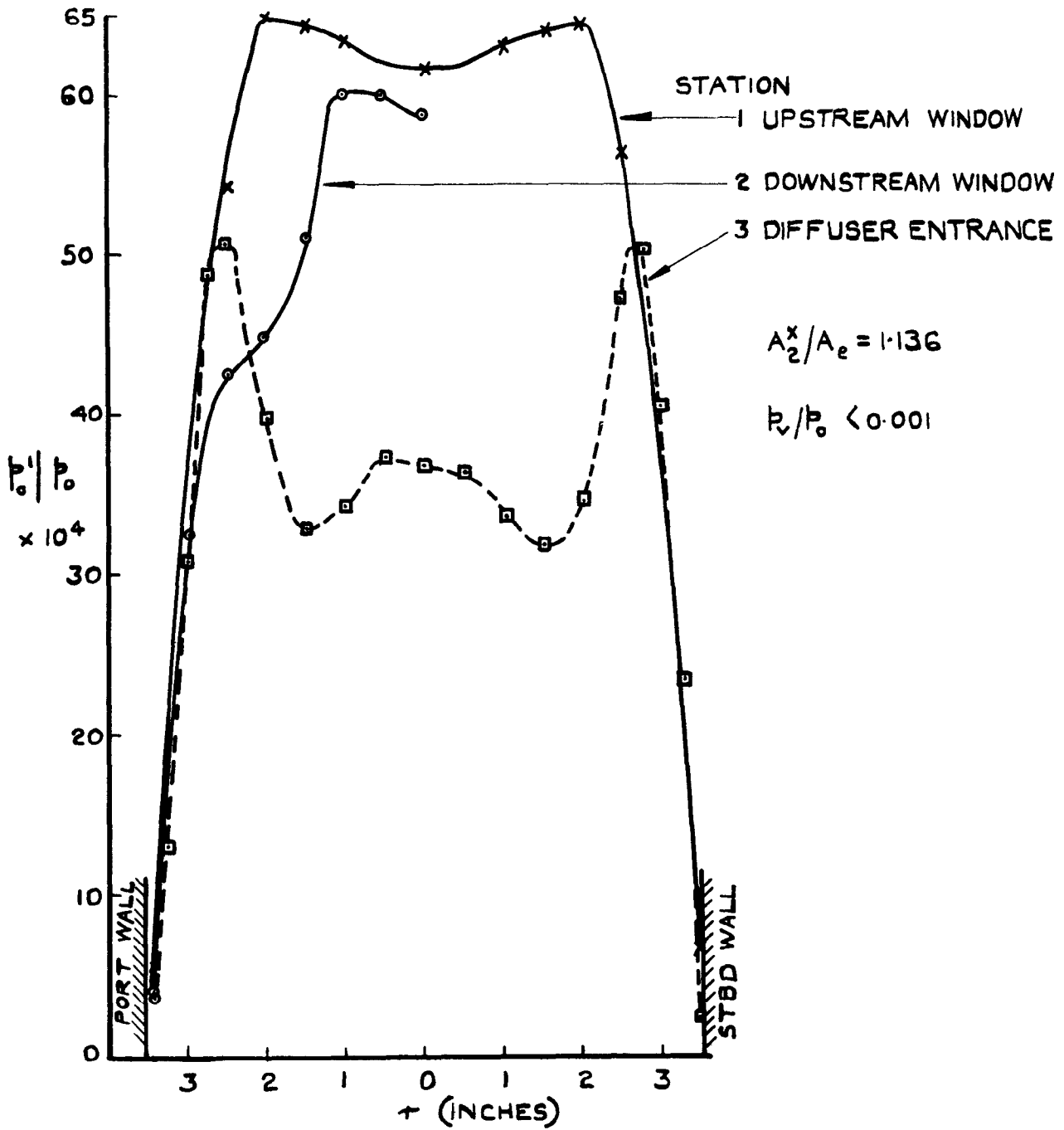
r (INCHES)
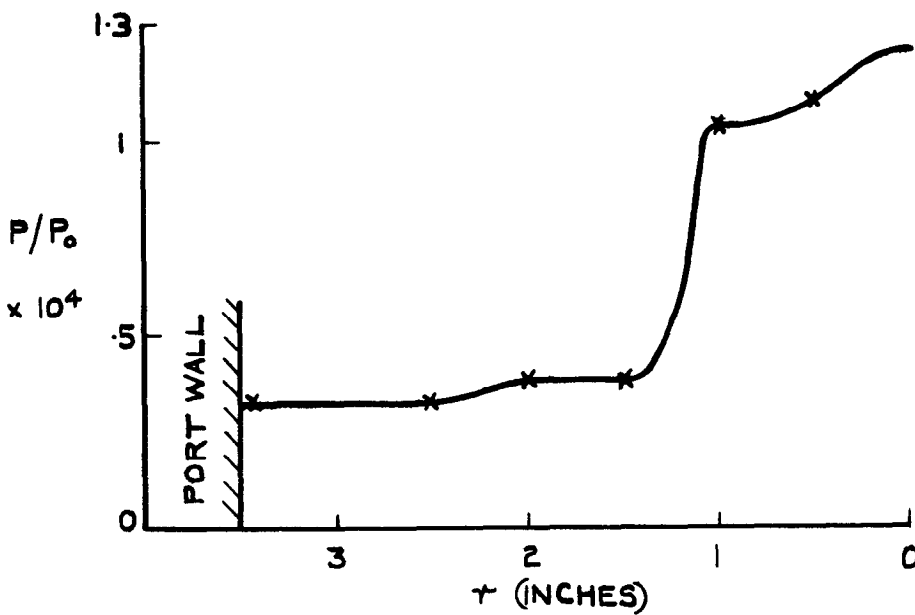
(b) STATIC PRESSURE PROFILE AT STATION 2.

FIG. 2. CALIBRATION OF THE EXPANDING JET.
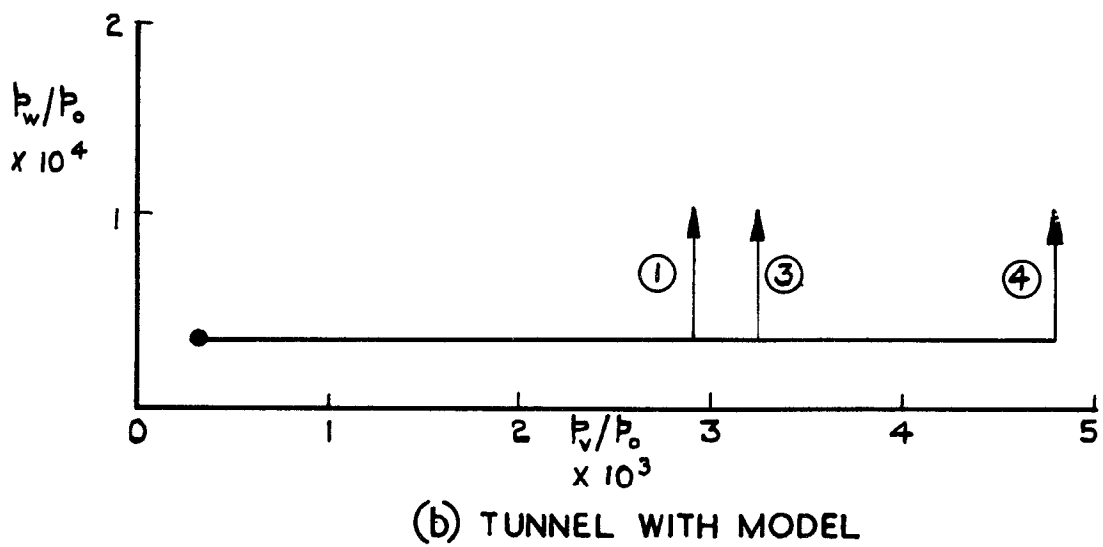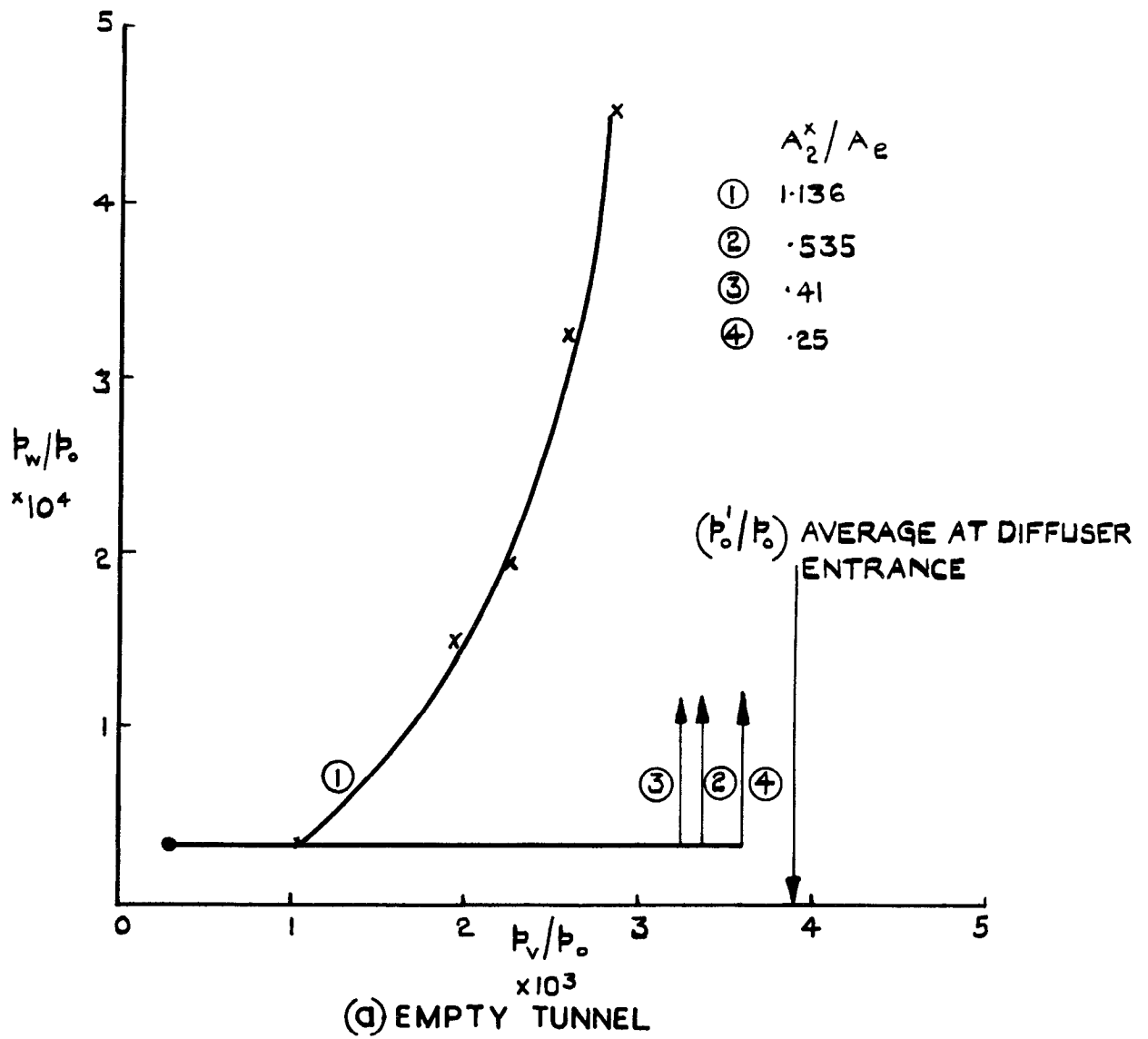
FIG.3. VARIATION OF WALL PRESSURE (STATION 2) WITH BACK PRESSURE FOR VARIOUS TUNNEL ARRANGEMENTS.
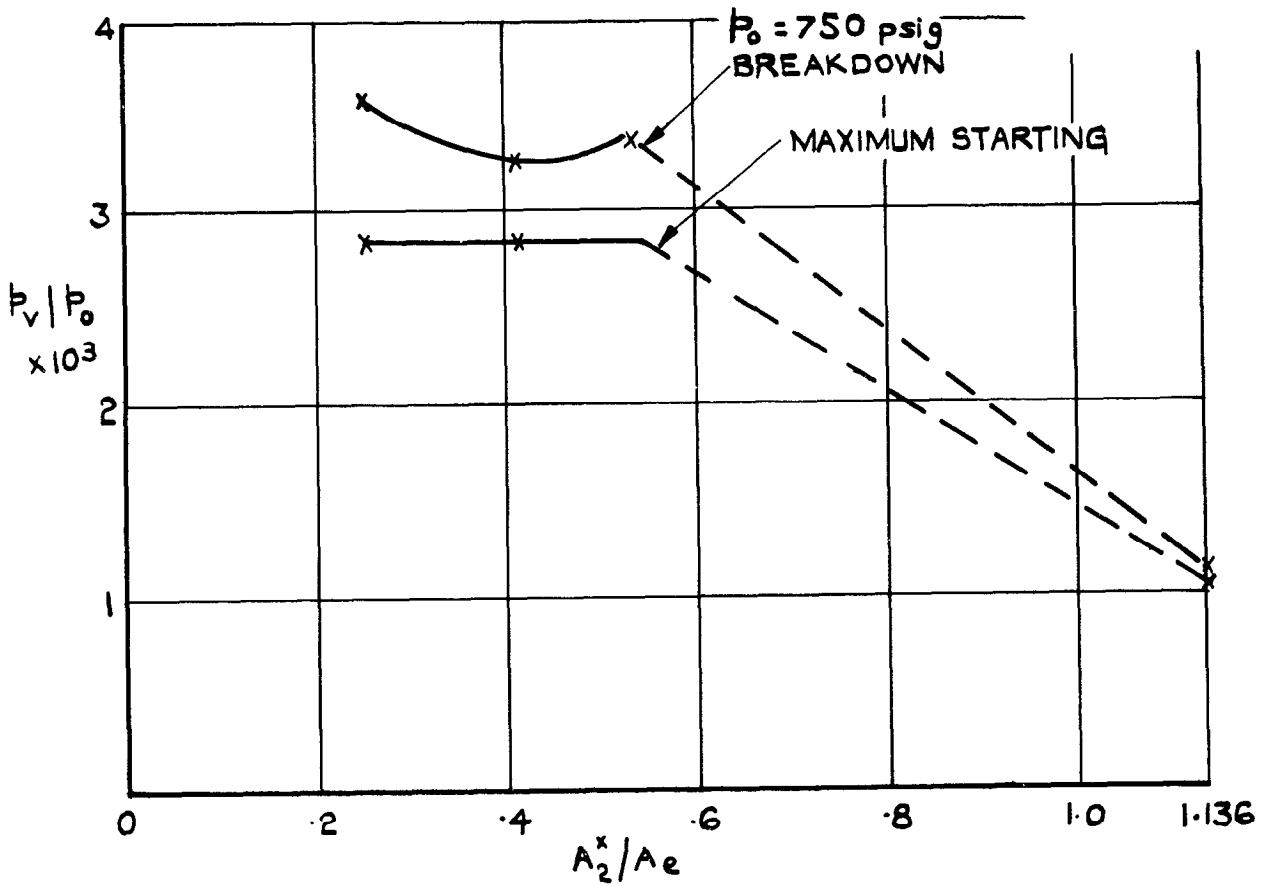
(a) EMPTY TUNNEL
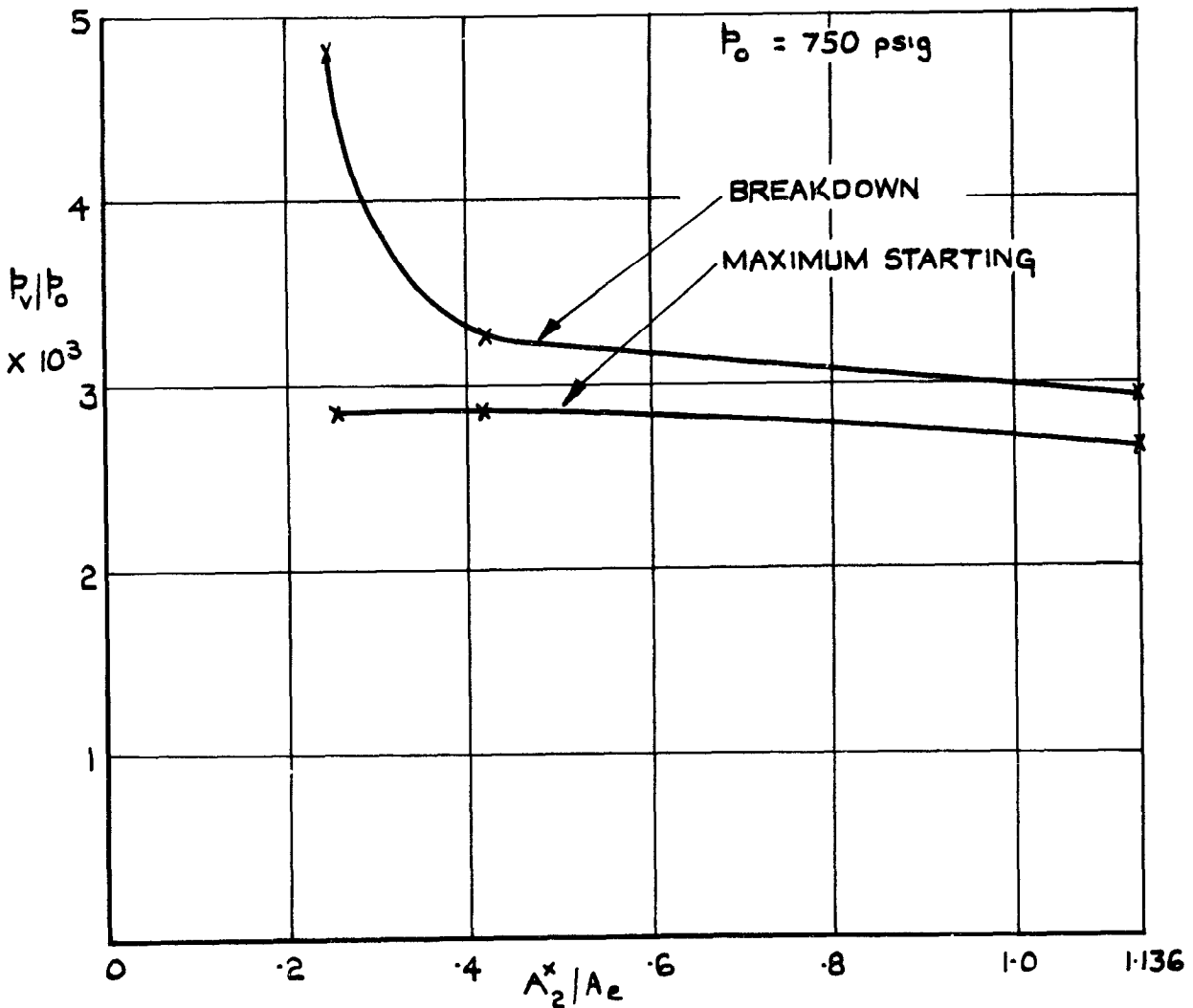
(b) TUNNEL WITH MODEL IN WORKING SECTION.

FIG. 4. MAXIMUM STARTING & BREAKDOWN PRESSURE RATIOS FOR AN EMPTY TUNNEL & FOR A TUNNEL WITH A MODEL IN THE WORKING SECTION.

X 750 } P₀ (psig)
⊙ 400

MINIMUM STARTING SIZES

0·527 AT P₀ = 750 psig
0·54 AT P₀ = 400 psig
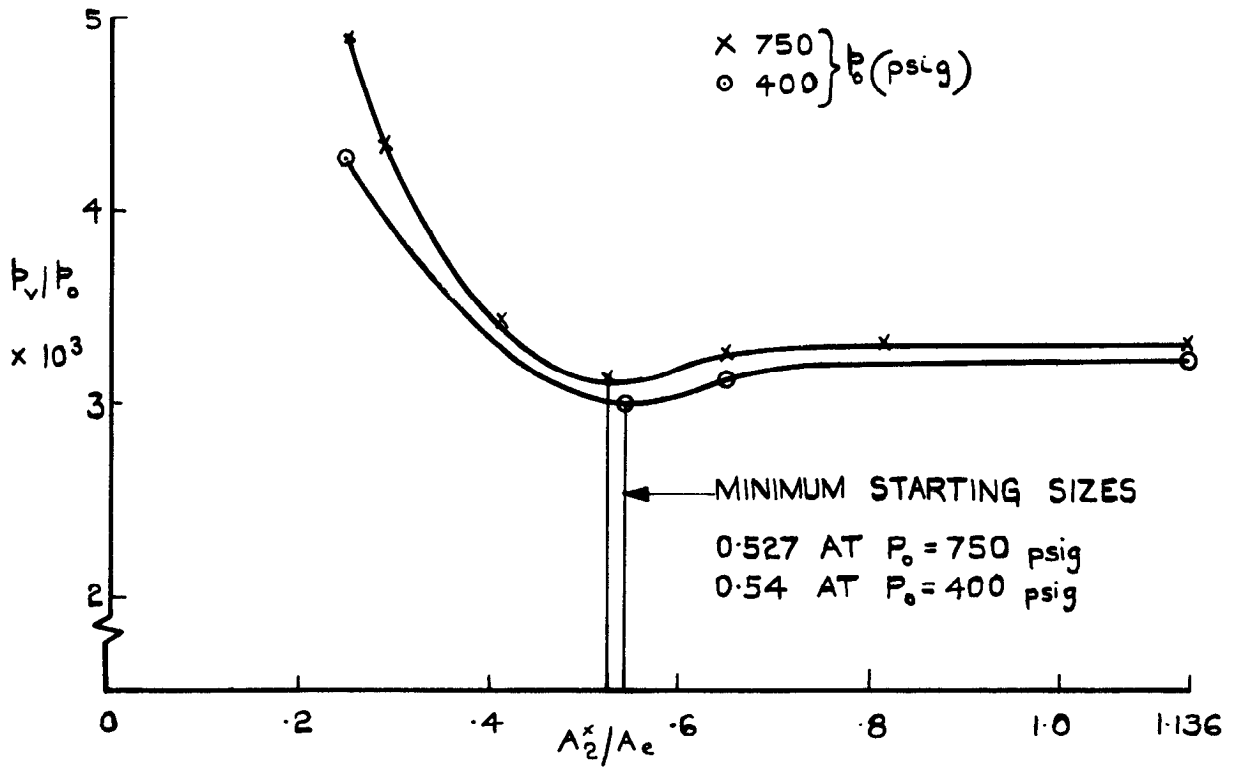
FIG.5.(a) EFFECT OF STAGNATION PRESSURE ON
BREAKDOWN PRESSURE RATIO
(SIGNAL FROM PITOT RAKE IN NOZZLE)

MODEL IN WORKING SECTION (P_w SIGNAL)
PITOT RAKE IN NOZZLE (P_o' SIGNAL)

EMPTY TUNNEL
(P_w SIGNAL)

P_o = 750 psig
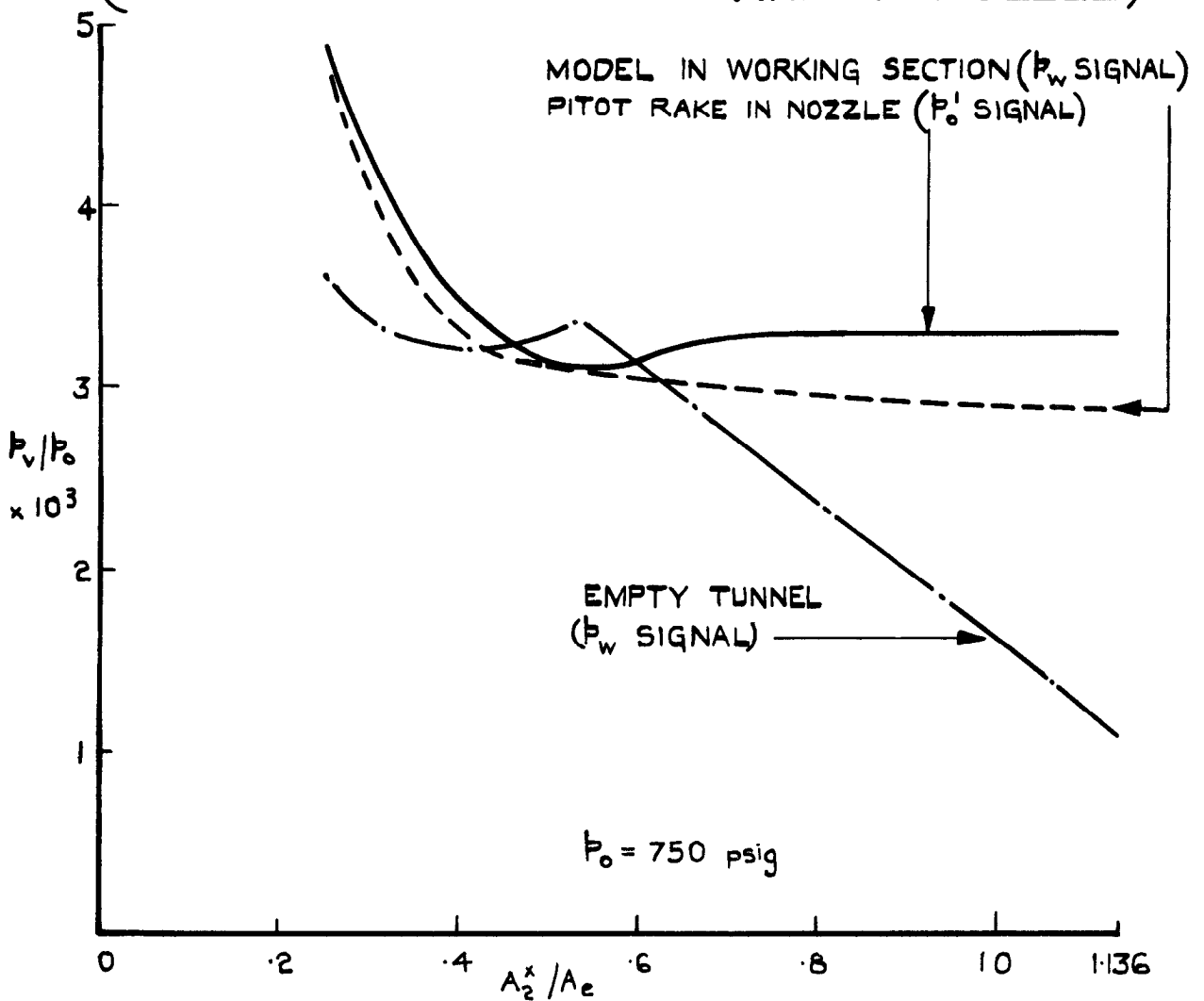
FIG. 5.(b) COMPARISON OF BREAKDOWN
CHARACTERISTICS FOR DIFFERENT
TUNNEL ARRANGEMENTS.
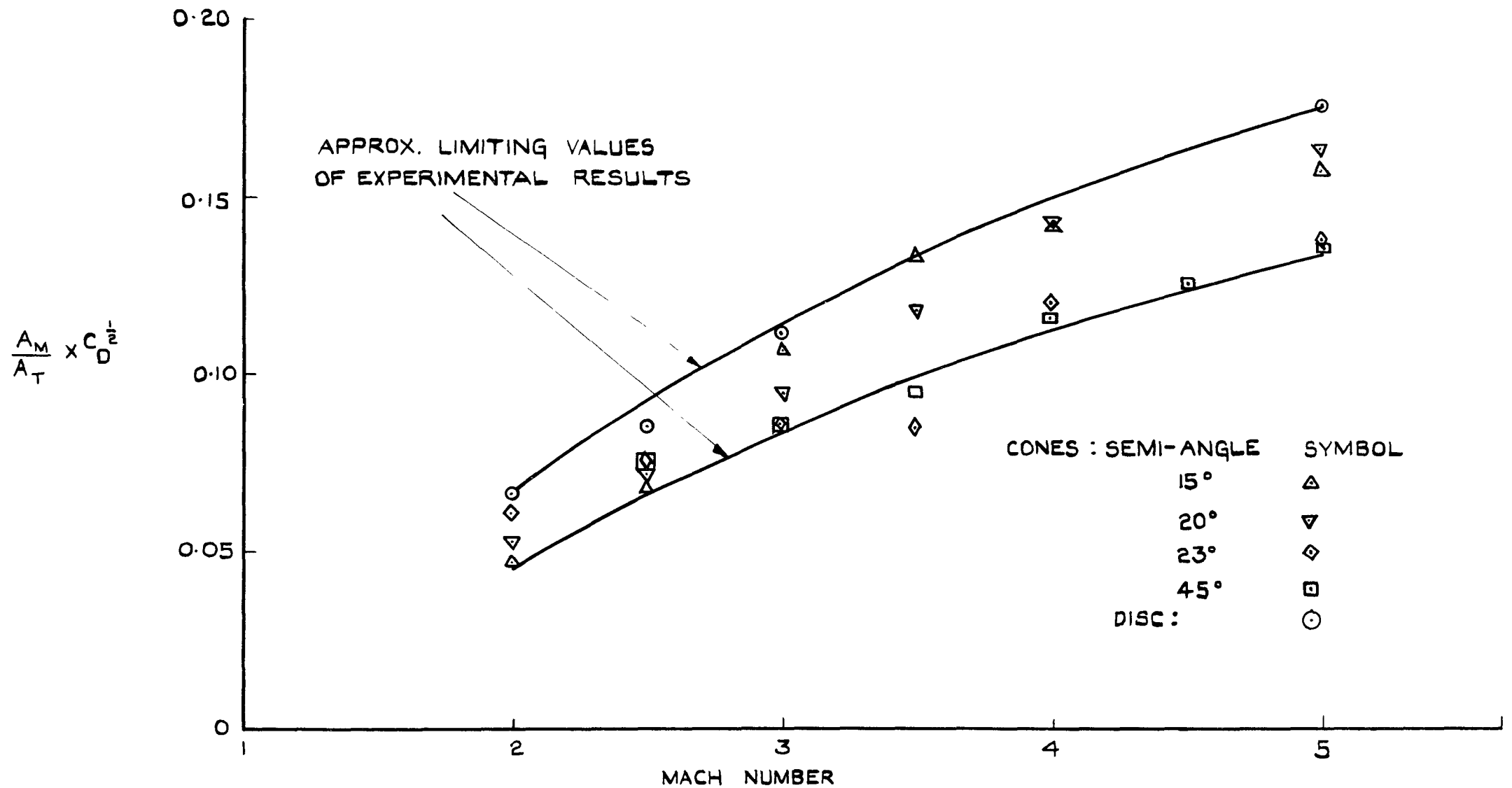
FIG. 6. CORRELATION OF BLOCKAGE AREA RATIO v MACH No FOR SCHUELERS RESULTS USING $C_D^{\frac{1}{2}}$ AS A WEIGHTING FACTOR.

LIMITING CURVES FOR RESULTS GIVEN IN FIG.6.

FLOW ESTABLISHMENT MARGINAL ⑧ ② ③

LOGARITHMIC EXTRAPOLATION

0.15

FLOW ESTABLISHED (MODEL SIZES NOT OPTIMUM) ⑦ ① ⑥

0.10

RESULTS FOR MODELS IN HYPERSONIC TUNNEL: Ⓝ
WHERE n DENOTES No. OF MODEL LISTED IN TABLE I.
RESULTS TAKEN FROM REF. 6

$\dfrac{A_M}{A_T} \times C_{D_0}^{\frac{1}{2}}$

SYMBOL	MODEL
△	14·6° CONE – CYLINDERS
▽	19·7° CONE – CYLINDERS
◇	27·6° TO 36·6° CONE- CYLINDERS
⊙	DISC
⌒	HEMISPHERE-CYLINDERS & SPHERES
OPEN SYMBOLS ~ START		
SOLID SYMBOLS ~ BLOCK		
HALF SOLID & HALF OPEN SYMBOLS ~MARGINAL		

⑤ ④

0.05

0

1   2   3   4   5   6   7

MACH NUMBER

FIG.7. COMPARISON OF THE TREND OF BLOCKAGE RESULTS FROM FIG.6. WITH THOSE OF REF. 6,& RESULTS FROM THE R.A.E. HYPERSONIC TUNNEL.

(a) STING.

MAX. DEPTH = $\frac{5}{16}$ AT BASE
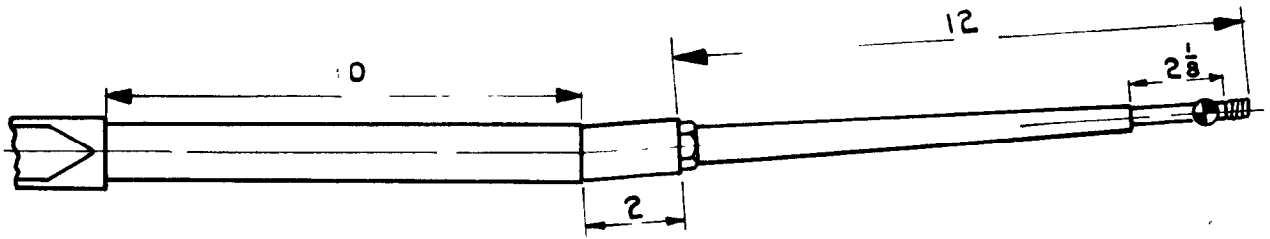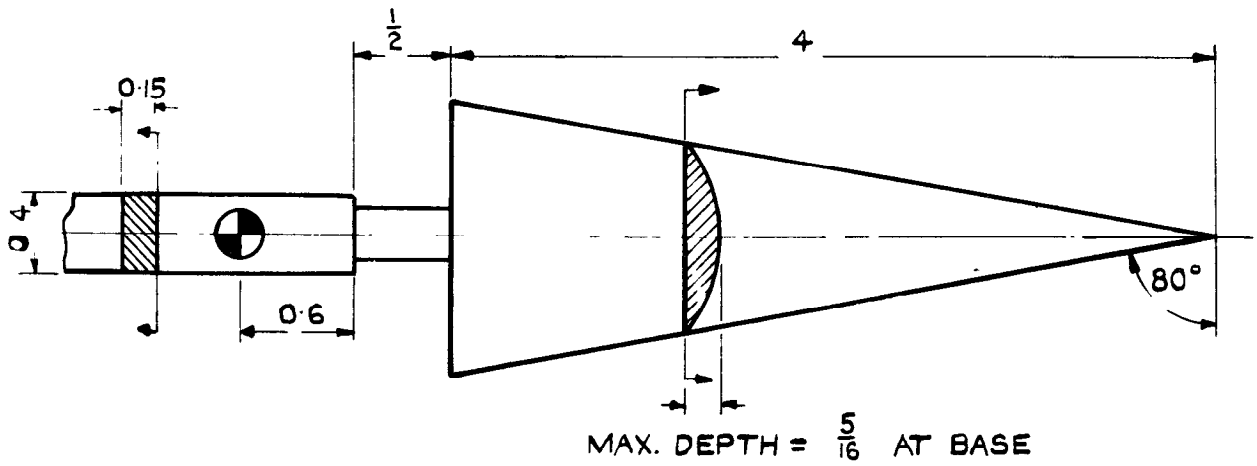
(b) DELTA WING MODEL.

⊕ BRIDGE CENTRE, DIMENSIONS IN INCHES
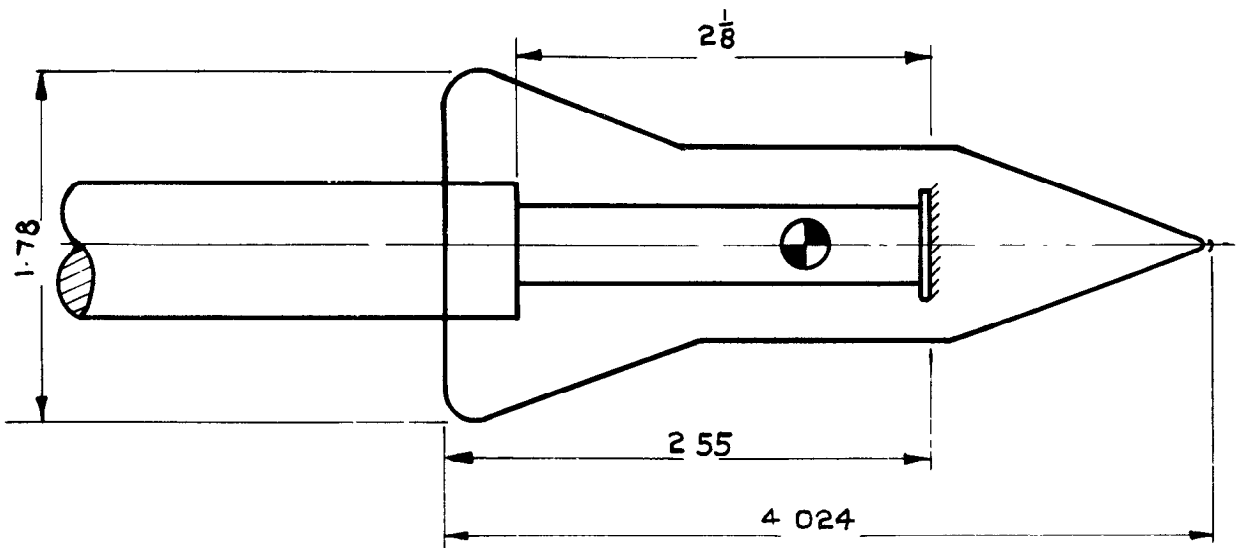
(c) CONE-CYLINDER-FLARE-MODEL

FIG.8. DETAILS OF MODELS USED FOR STARTING LOAD MEASUREMENTS.

STRAIN GAUGE BRIDGES

NORMAL
FORCE

MOMENT

V_i = 4 VOLTS

Z

M'

50Ω

250Ω

250Ω

R_G = 40Ω

R_G = 40Ω

GALVANOMETER TYPE G 227/124 (OIL DAMPED)
12 CHANNEL RECORDER TYPE LT. 1-11.
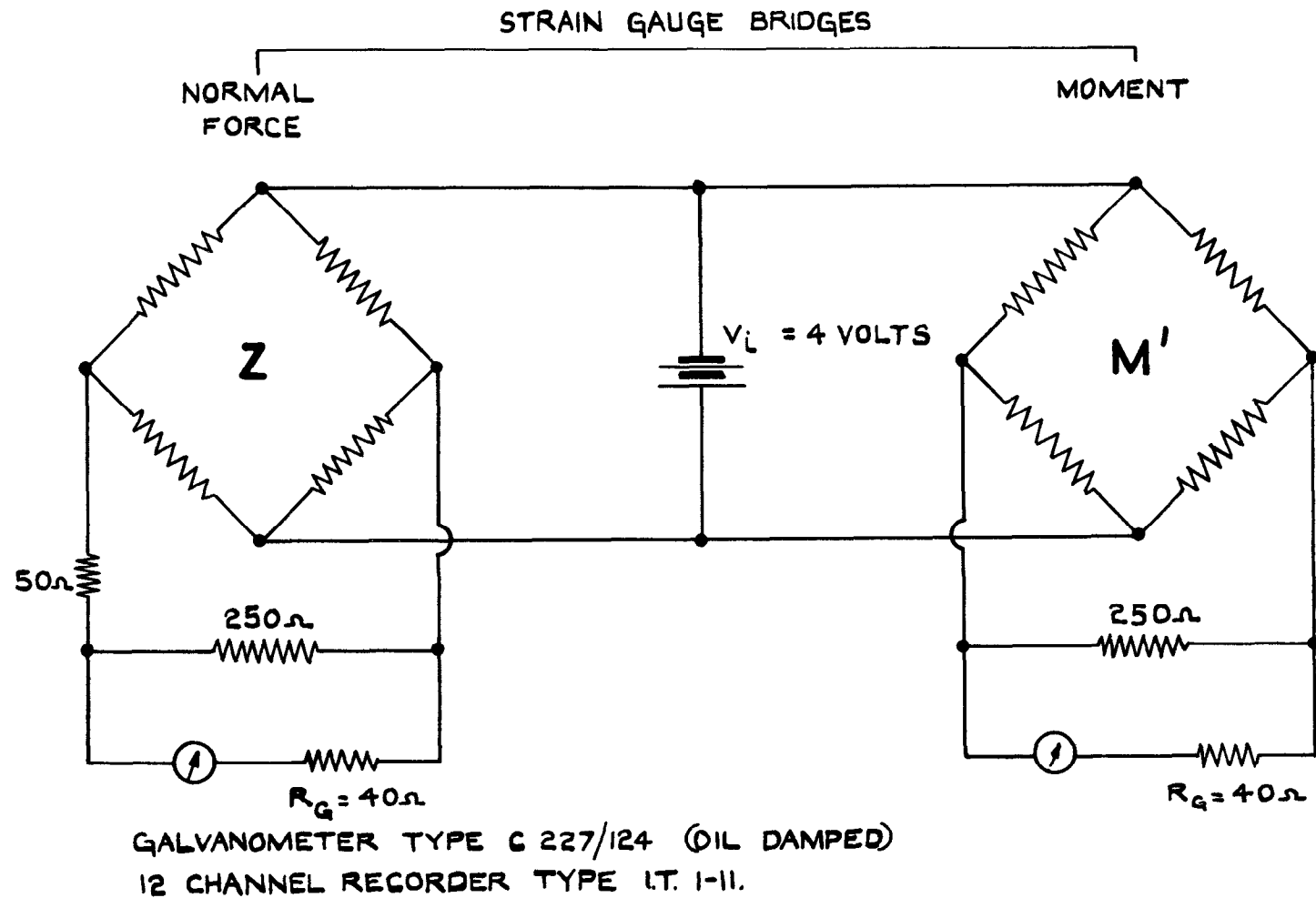
FIG.9. D.C. BRIDGE CIRCUIT USED FOR RECORDING LOADS DURING STARTING.
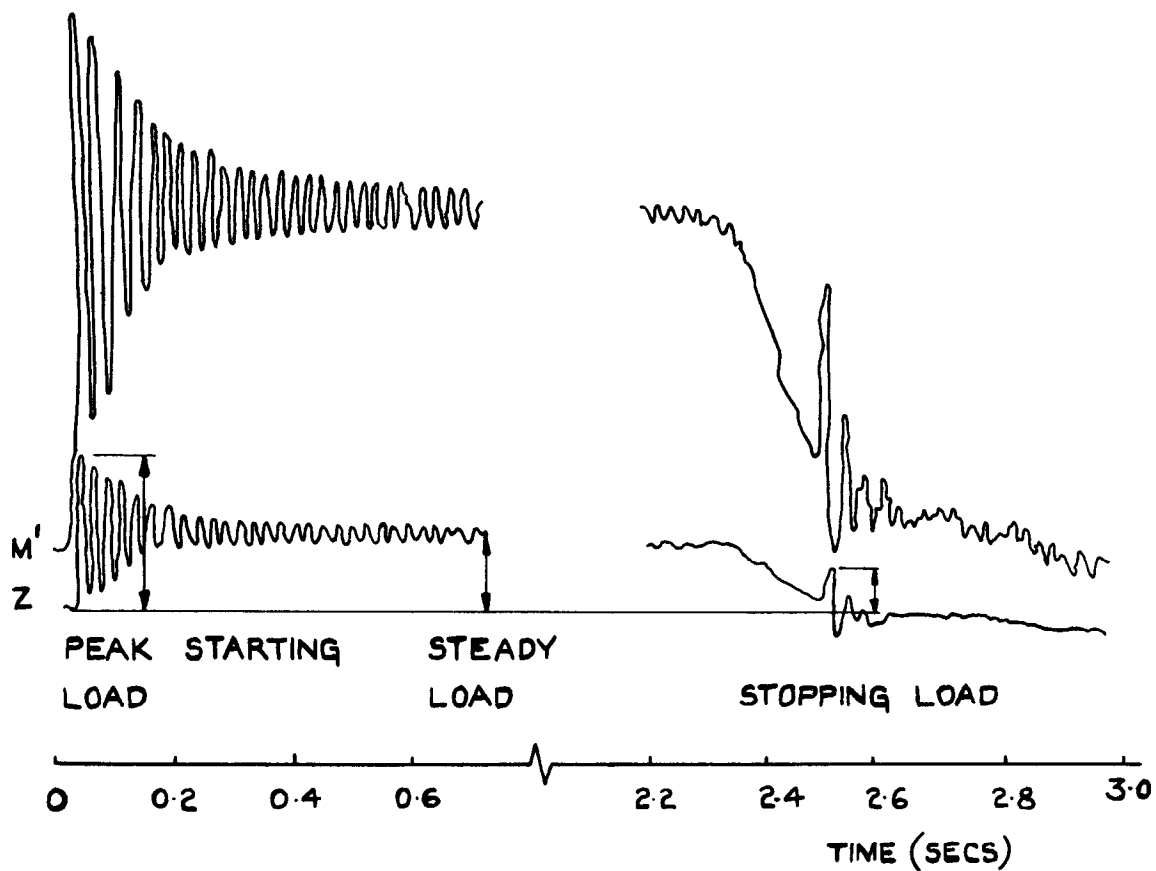
(a) $p_V = 0.2$ ATMOSPHERES
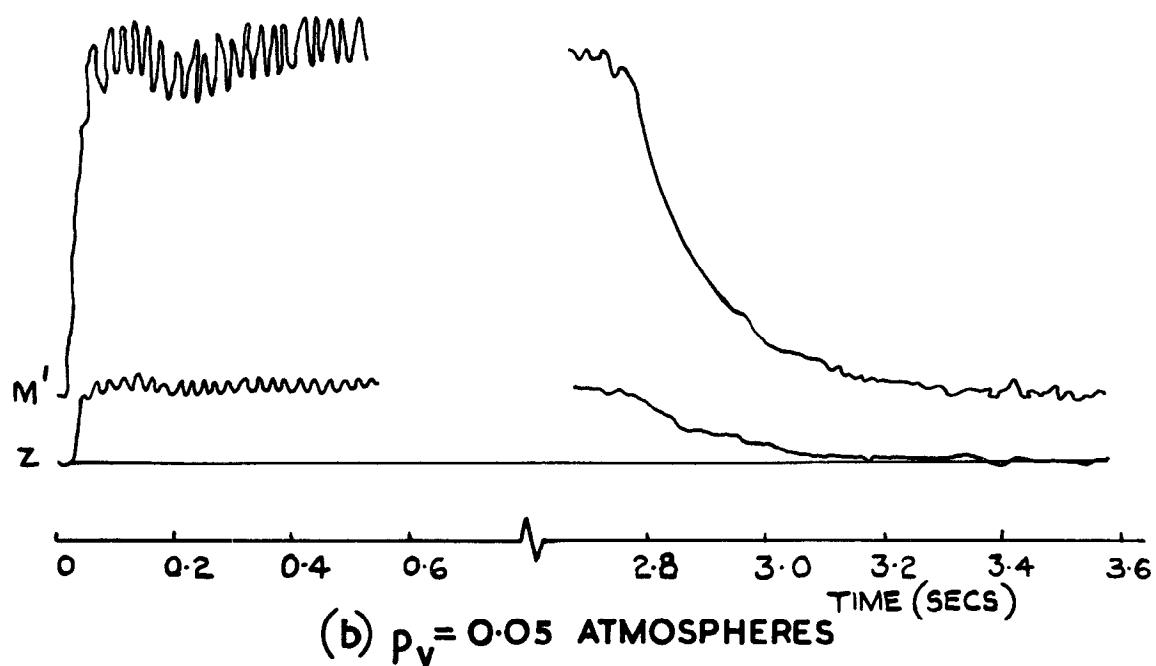
(b) $p_V = 0.05$ ATMOSPHERES

FIG.IO. GALVANOMETER TRACES SHOWING
VARIATION OF STARTING LOAD WITH VACUUM TANK
PRESSURE, p_V (DELTA WING MODEL AT 4° INCIDENCE.)
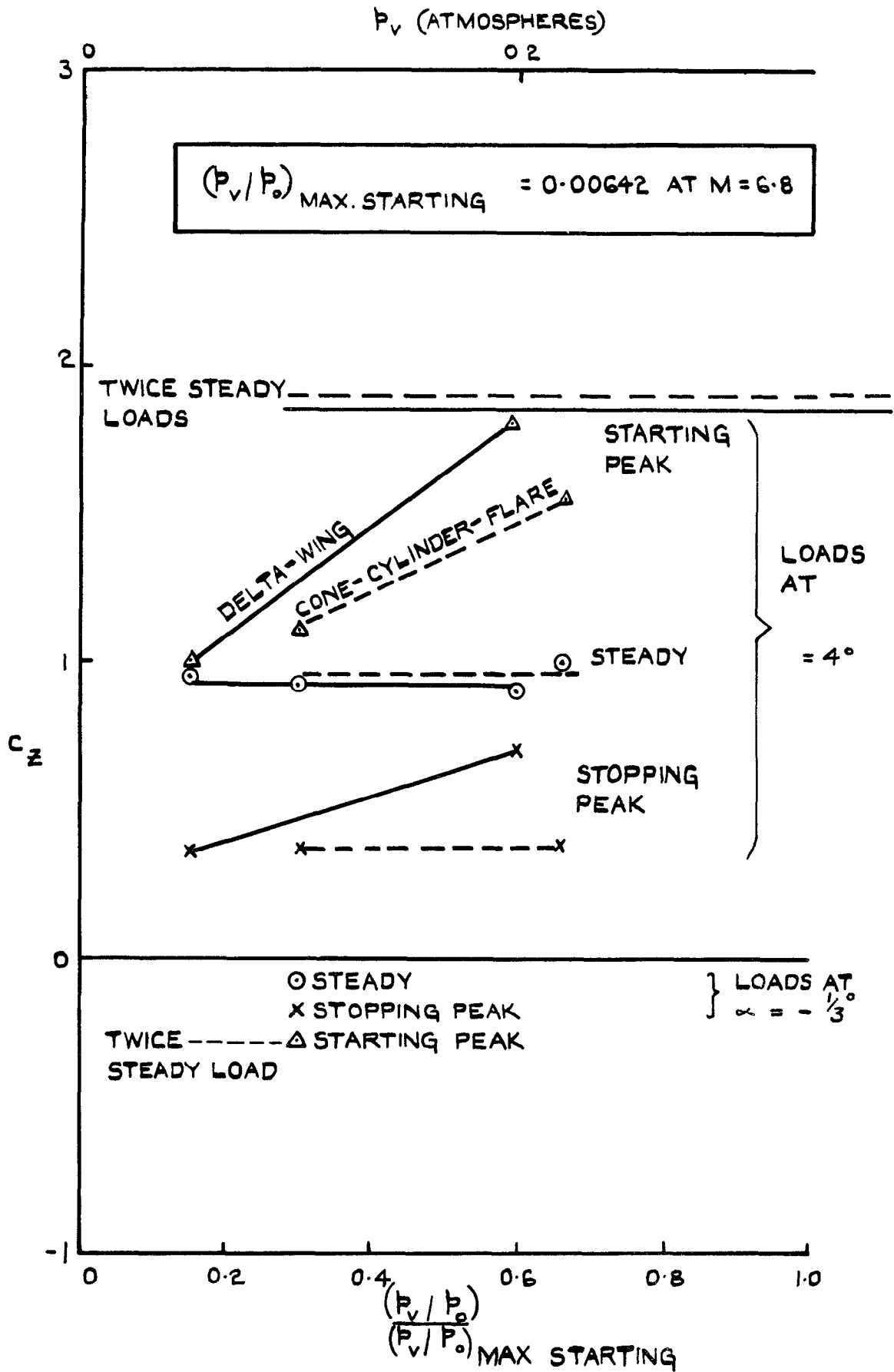
FIG.11. EFFECT OF VACUUM TANK PRESSURE, P_v, ON STARTING AND STOPPING LOADS ON MODELS AT M=6·8.

A.R.C. C.P. No.663

533.6.071.1.011.55:
533.6.071.5.011.55

THE 7 IN. X 7 IN. HYPERSONIC WIND TUNNEL AT R.A.E. FARNBOROUGH PART IV —
MEASUREMENTS OF DIFFUSER PERFORMANCE, BLOCKAGE, STARTING LOADS AND
HUMIDITY.   Crane, J. F. W. and Woodley, J. G.   December, 1962.

The performance of the diffuser is analysed, (a) for a conventional
closed-jet tunnel with a two-dimensional M = 7 nozzle, and (b) for a type of
free-jet tunnel resulting from the combination of an axisymmetric M = 8.6
nozzle and a two-dimensional working section.
    Some results of model blockage are given together with a new correla-
tion of closed-jet tunnel results.
    Starting loads measured on two models show that the load varies with
back pressure and may be reduced to insignificant size.
    Humidity measurements show that the technique of drying-by-compression
is satisfactory.

.

.